

Unraveling the structural stability and the electronic structure of ThO₂ clusters Electronic Supplementary Information (ESI)

Néstor F. Aguirre,^{‡§} Julie Jung,^{‡§} and Ping Yang^{§*}

Contents

S1 Geometry Search	S1
S1.1 Choice of Building-Blocks	S1
S1.2 Geometry Optimization	S2
S1.3 Dataset	S3
S2 Singlet-Triplet energy differences	S4
S3 DOS and HOMO-LUMO gap	S5
S4 Detailed Description of the Lowest Energy Structures, and Some of Their Isomers	S6
S4.1 ThO ₂	S6
S4.2 Th ₂ O ₄	S8
S4.3 Th ₃ O ₆	S8
S4.4 Th ₄ O ₈	S9
S4.5 Th ₅ O ₁₀	S9
S4.6 Th ₆ O ₁₂	S10
S4.7 Th ₇ O ₁₄	S10
S4.8 Th ₈ O ₁₆	S11
S5 Stable isomers for the [Th₆(OH)₄(O)₄(O)₆] cluster	S13

[‡]NFA and JJ contributed equally

[§]Theoretical Division, Los Alamos National Laboratory, Los Alamos, New Mexico
87545, United States

*E-mail: pyang@lanl.gov

S1 Geometry Search

S1.1 Choice of Building-Blocks

This approach is chemically-driven in the sense that the elementary units used to build the clusters are entire ThO_2 molecules. This choice is motivated by the infra-red study of thorium oxide species by Andrews *et al.* as it shows that stoichiometric ThO_2 clusters are predominantly formed in an oxygen-rich conditions. In the first step of the geometry search approach, the set of initial structures is generated from the repetition of one or more building-blocks. In the present work, depending on the size of the Th_nO_{2n} clusters, different building-blocks are used to ensure thorough sampling of the potential energy surface. For the clusters with $n = 1 - 4$, simple atoms are used, and all possible combinations of n thorium atoms and $2n$ oxygen atoms are considered. Due to the large number of possible combinations, this strategy becomes impractical for the clusters with $n = 5$, and beyond. Thus, for the clusters with $n = 4 - 5$, a new strategy is used: now, entire ThO_2 molecules are used as building-blocks (or units). They correspond to the three ThO_2 isomers identified as stable from the previous strategy. This strategy exploits the fact that, in the clusters with $n = 1 - 4$, all thorium atoms are connected to one or more oxygen atoms. In order to guarantee the stability and the continuity of the two strategies, the clusters with $n = 4$ are investigated using both methods. The two strategies yield identical sets of structures, which validates the use of ThO_2 molecules as building blocks (or units). However, from $n = 6$, this new strategy becomes impractical again, as it fails to converge. By definition, convergence is reached when a new run of the search algorithm only generates structures that already exist. Since the number of possible structures increases exponentially with increasing cluster size, when the search strategy is not adapted to the size of the system anymore, it is expected fail. And this is exactly what happens for the the clusters with $n = 6$, when using entire ThO_2 molecules as building blocks. Hence, a nucleation inspired strategy is used: the new structures are now built by adding ThO_2 molecules (building units) to the low energy structures of the $\text{Th}_{(n-1)}\text{O}_{2(n-1)}$ series. Typically, all identified structures within the first 1 eV above the lowest energy structure are considered. The validity of this new method is evidenced by $n = 6$, which are searched by both methods yielding the same set of minima structures.

Strictly speaking, the molecular and the nucleation strategies are not global optimization procedures. However, they can be considered as such because they give rise to the same set minimum energy structures for the clusters series where two different approaches are used.

S1.2 Geometry Optimization

All structures generated by the above search algorithms are fully optimized at the DFT/PBE level of theory, using the ADF (Amsterdam Density Functional, v2017) suite of programs.¹⁻³ Triple-zeta (TZP) ZORA basis sets are used in combination with large core effective potentials (i.e. O:1s², Th:[Xe]4f¹⁴5d¹⁰). Indeed, the ‘‘PBE/Large Core’’ combination shows the best compromise in terms of accuracy and computational cost, as shown from benchmark calculations carried out for the ‘‘PBE/Small Core’’ and ‘‘hybrid/Large Core’’ combinations. The results show that the geometry changes are less than 0.05 Å and the stabilization energy changes, less than 0.2 eV (Tab. S1-S3). However the computational cost increases by a factor of 2-to-3 for small core ECPs (i.e. O:1s², Th:[Kr]4d¹⁰4f¹⁴), and a factor of 50 for hybrid functionals. Scalar relativistic effects are accounted for by using the zeroth-order regular approximation (ZORA) Hamiltonian.⁴⁻⁸ Energy convergence is achieved to 10⁻⁵ Eh, and geometry convergence, to 10⁻⁴ Å. Frequency calculations are carried out at the harmonic level approximation with no correction, in order to ensure that the optimized structures are located at global or local minima on the potential energy surface. Additionally, all computed final energies are corrected for zero-point energies (ZPE) derived from the harmonic frequency analysis.

	ThO ₂	Th ₂ O ₄	Th ₃ O ₆	Th ₄ O ₈	Th ₅ O ₁₀	Th ₆ O ₁₂
PBE/Small Core	0.002	0.002	0.002	0.003	0.002	0.002
PBE/Large Core	0.000	0.000	0.000	0.000	0.000	0.000
PBE0/Small Core	0.012	0.013	0.027	0.011	0.015	0.012
PBE0/Large Core	0.031	0.015	0.025	0.013	0.011	0.017
B3LYP/Small Core	0.006	0.012	0.018	0.014	0.020	0.021
B3LYP/Large Core	0.027	0.020	0.049	0.031	0.034	0.035

Table S1: Geometry changes in Å, provided as RMSD after coordinates are translated and rotated using quaternions [W. Walker, Lejun Shao, and Richard. *CVGIP: Image Understanding*, **54**, 358-367 (1991). Implementation: <http://github.com/charnley/rmsd>]. The changes are provided with respect to the ‘PBE/Large Core’ description. The largest distortions are bolded.

	ThO ₂	Th ₂ O ₄	Th ₃ O ₆	Th ₄ O ₈	Th ₅ O ₁₀	Th ₆ O ₁₂
PBE/Small Core	0.00	-1.96	-2.79	-3.29	-3.72	-3.96
PBE/Large Core	0.00	-1.97	-2.82	-3.32	-3.75	-4.00
PBE0/Small Core	0.00	-2.07	-2.95	-3.52	-3.97	-4.25
PBE0/Large Core	0.00	-2.23	-3.18	-3.79	-4.28	-4.59
B3LYP/Small Core	0.00	-2.02	-2.81	-3.40	-3.77	-4.05
B3LYP/Large Core	0.00	-2.15	-2.99	-3.62	-4.02	-4.32

Table S2: Stabilization energy in eV (see footnote in main text for the definition of stabilization energy).

	ThO ₂	Th ₂ O ₄	Th ₃ O ₆	Th ₄ O ₈	Th ₅ O ₁₀	Th ₆ O ₁₂
PBE/Small Core	3.0	2.2	2.9	2.3	2.5	2.1
PBE/Large Core	1.0	1.0	1.0	1.0	1.0	1.0
PBE0/Small Core	78.0	121.5	130.8	134.3	113.0	108.0
PBE0/Large Core	56.4	96.0	84.7	88.1	35.4	70.7
B3LYP/Small Core	68.9	108.1	93.7	106.5	79.7	87.8
B3LYP/Large Core	58.2	91.3	86.9	88.2	70.0	66.8

Table S3: Relative computational cost for the geometry optimization (CPU time per geometry optimization iteration), with respect to the ‘PBE/Large Core’ description.

S1.3 Dataset

For each series of cluster ranging from ThO_2 to Th_8O_{16} , Figure S1 shows the distribution of the stable structures obtained from the geometry search approach discussed above and in the main text. From the computational perspective, stable structures are characterized by non imaginary frequencies.

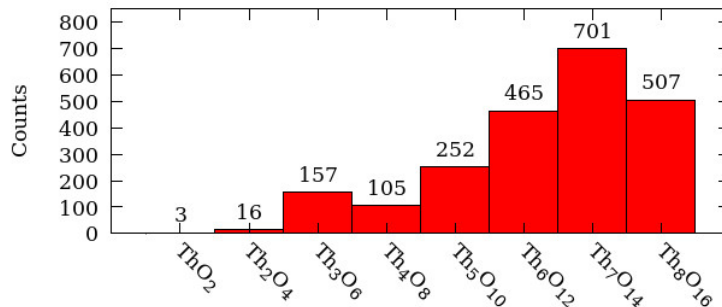


Figure S1: Distribution of the stable structures for each size of cluster

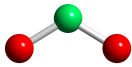
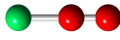
The complete set of structures generated in this work together with their symmetry, relative energy (including ZPE correction) (in eV) and file name are provided in the **geometries.pdf** file included in the geometries-ThnO2n.zip file, in addition to the ESI†. File names obey the following format: <stoichiometry>.q<charge>.m<multiplicity>-<id>. All structures in the .xyz format are also available in a supplementary file (geometries-ThnO2n.zip). Figure S2 shows the typical structure of these .xyz files which is the standard format used by M3C.

```
1 3
2 Energy = -0.81319249
3 Th      0.000000    0.000000    0.759044
4 O       0.000000    1.637789   -0.232439
5 O       0.000000   -1.637789   -0.232439
6
7 FREQUENCIES 3
8 153.628463
9 764.030301
10 809.174900
11
12 SYMMETRY C2V
```

Figure S2: line 1: number of atoms n , line 2: total energy in a.u., lines 3-5: symbols and positions in Å of the atoms contained in the cluster, line 7: comment, lines 8-10: vibrational frequencies in cm^{-1} , and line 12: symmetry.

S2 Singlet-Triplet energy differences

Table S4: Energy difference (eV) between the lowest triplet and singlet isomers of the ThO₂ molecule computed at the DFT and CCSD(T) level of theory, using all electron basis sets: $\Delta E = E(T) - E(S)$

Isomer	1	2	3
			
PBE	2.18	0.58	0.38
PBE0	2.37	0.70	0.31
B3LYP	2.29	0.83	0.53
CCSD(T)	2.30	1.69	0.91

The aforementioned all-electron DFT and coupled-cluster calculations were performed with the quantum chemistry package ORCA 4.0.1.⁹ These calculations used the all-electron DEF2-TZVPP basis set for oxygen^{10,11} and the all-electron SARC-TZVPP basis set for thorium.¹² Scalar relativistic effects were accounted for by using of the zeroth-order regular approximation (ZORA) Hamiltonian. Convergence was achieved towards VERYTIGHTSCF settings, i.e. energy change to 1e-9 Eh, max density change to 1e-8, RMS density change to 1e-9, orbital gradient to 2e-6 and orbital rotation angle to 2e-6. SCF convergence was achieved using the DIIS algorithm for the first 10-15 SCF iterations, and then the more accurate NRSCF algorithm. The DFT calculations made use of the PBE, PBE0 and B3LYP functionals. The RI approximation (RI and RIJONX, for GGA and hybrid functionals, respectively) was used to speed up the calculations, in combination with the DEF2/J and SARC/J auxiliary basis sets. Additionally, the accuracy of the Lebedev770 integration grid was further increased in the surrounding of the thorium atom (intacc=9), for better convergence. All the coupled-cluster calculations were performed at the CCSD(T) level of theory, i.e. including the singles and doubles explicitly, and triples perturbatively.

S3 DOS and HOMO-LUMO gap

Structure	HOMO				LUMO		Δ
	O-2p	Th-5f	Th-6d	Th-6p	Th-7s	Th-7p	
ThO ₂	72	15	7	8	74	9	2.33
Th ₂ O ₄	75	6	5	3	74	6	2.98
Th ₃ O ₆	69	7	9	7	73	11	2.59
Th ₄ O ₈	66	10	8	8	77	5	2.18
Th ₅ O ₁₀	68	6	9	6	61	17	2.44
Th ₆ O ₁₂	89				73	10	3.34
Th ₇ O ₁₄	84				70	7	3.27
Th ₈ O ₁₆	82				65	6	3.31

Table S5: Dominant contributions to the HOMO and LUMO (in %), together with HOMO-LUMO gap, Δ (in eV), for the lowest energy structure of each cluster ranging from ThO₂ to Th₈O₁₆

	HOMO					LUMO					Δ
	O-2p	Th-6s	Th-6p	Th-5f	Th-6d	O-2p	Th-5f	Th-6d	Th-7s	Th-7p	
1	71		8	14	7			14	74	8	2.33
2		77			15	17	54	27			0.63
3	(82)			(5)	(11)						
		86			11		30	70			0.83

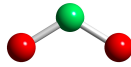
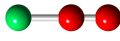
Table S6: Dominant contributions to the HOMO and LUMO (in %), together with HOMO-LUMO gap, Δ (in eV), for the three ThO₂ isomers. The values in parenthesis correspond to the HOMO-1 for isomer **3**. The latter is almost degenerate with the HOMO ($\Delta E = 0.126$ eV), and gives rise to the oxygen peak close to the Fermi level, as shown in Fig. 4.

S4 Detailed Description of the Lowest Energy Structures, and Some of Their Isomers

S4.1 ThO₂

For the thorium dioxide molecule ThO₂, the geometry search algorithm evidences three stable singlet isomers (Tab. S7). As expected from the work by Wadt,¹³ the minimum energy structure (isomer **1**) presents a bent structure with C_{2v} symmetry. The Th-O and O-O bond distances are 1.92 Å and 3.28 Å, respectively, and the O-Th-O angle, 117.6 °. The next stable structure (isomer **2**) is found 5.21 eV higher in energy than isomer **1**. It is very similar to isomer **1**: while it also has a bent structure with C_{2v} symmetry, the O-Th-O angle is significantly smaller (42.0 ° vs. 117.6 °), resulting in a significantly shorter O-O distance (1.51 Å vs 3.28 Å), and slightly longer Th-O bond distances (2.08 Å vs. 1.92 Å). This O-O distance is close to the characteristic bond distance in the O₂²⁻ peroxido group (i.e. 1.49 Å). Finally, the last structure (isomer **3**) is found 7.27 eV higher in energy than isomer **1**. It is very different from both isomer **1** and isomer **2**: with a O-Th-O angle of 0.0 °, isomer **3** is linear (C_{∞v} symmetry). Its Th-O and O-O bond distances are 1.94 Å and 1.36 Å, respectively, which is in the range of the previously reported Th-O distances for the first, but shorter than any O-O distance reported so far, for the second. This O-O distance is very close to to the characteristic bond distance in the O₂⁻ radical superoxido group (i.e. 1.34Å).¹⁴ Furthermore, each of the aforementioned isomers possesses a triplet analogue higher in energy (Tab. S7). In each case, the structure of both the lowest singlet and the lowest triplet states are fully optimized. The lowest singlet state is always found lower in energy than the lowest triplet state, but both keep the same structural features.

Table S7: Structural, electronic and energetic characteristics of the three ThO₂ isomers

Isomer	1	2	3
			
Symmetry	C _{2v}	C _{2v}	C _{∞v}
d _{Th-O} (Å)	1.92	2.08	1.94
d _{O-O} (Å)	3.28	1.51	1.36
O - Th - O (°)	117.6	42.0	0.0
ΔE (eV)	0.0	5.21	7.27
ΔE _{S-T} (eV)	2.18	0.58	0.38

The structural changes observed in isomer **2** compared to isomer **1** are in line with that observed in their simulated IR spectrum (Fig. S3): while the stretching modes are shifted towards lower frequencies (578.8 cm⁻¹ vs. 809.2 cm⁻¹, and 528.4 cm⁻¹ vs. 764.0 cm⁻¹, respectively) and with inverted intensities, the bending mode, which can also be read as O-O stretching mode, is shifted towards higher frequency (870.0 cm⁻¹ vs. 153.6 cm⁻¹). Similarly, the structural changes observed in isomer **3** with respect to isomer **2** are reflected by the IR spectrum (Fig. S3): while the O-O stretching mode is shift towards higher frequency (1036.7 cm⁻¹ vs. 870.0 cm⁻¹), the Th-O stretching mode is shifted to even lower frequency (509.3 cm⁻¹ vs. 578.8 cm⁻¹) loosing even more of its intensity. Additionally, the weak Th-O-O bending mode that arises at 228.9 cm⁻¹ reflects the rigidity of the axial structure.

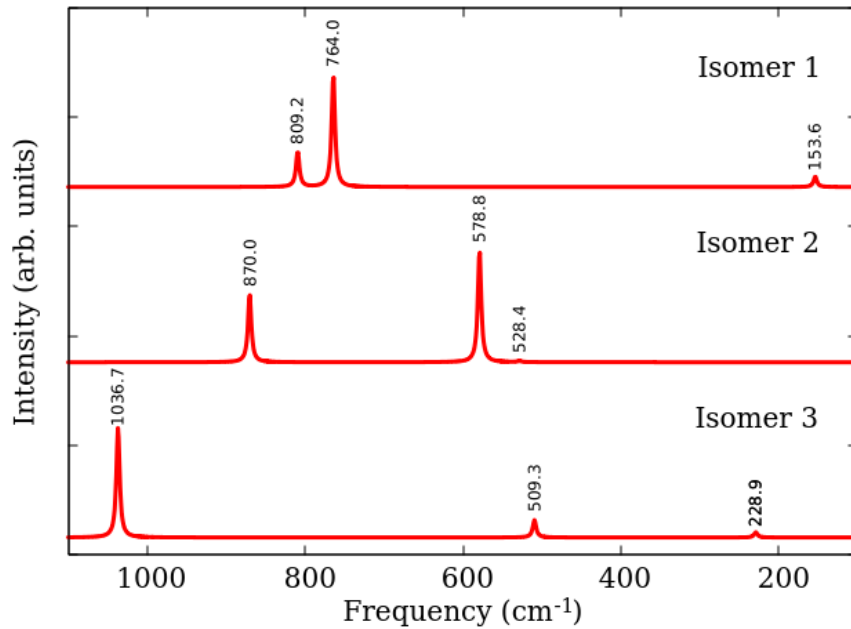


Figure S3: Simulated IR spectra for isomers **1-3** of ThO₂.

The IR active mode computed for isomer **1** compare well to previously reported values, both from experimental and theoretical works (Table S8). Typically, the shift to higher frequencies with respect to some experimental values can be attributed to the matrix in which the measurements are performed, which is known to affect the position of the active modes.¹⁵

Method	PP / Basis	ν_s	ν_{as}	ν_b	Ref.
PBE	(78/2)+TZP	809.2	764.0	153.6	<i>This work</i>
PW91	(78/2)+TZP	812	759	157	[16]
CCSD(T)	(78/2)+TZP	807.7	756.0	165.3	[15]
Dirac-Hartree-Fock	AE+DZP	896	761	139	[17]
Method	Matrix	ν_s	ν_{as}	ν_b	Ref.
Exp.	Argon	787	736	135	[18]
Exp.	Argon	787.4	735.3		[19]
Exp.	Argon	787.1	735.1		[15]
Exp.	Neon	801.7	748.1		[20]
Exp.	Neon	808.4	756.8		[16]
Exp.	Neon	808.7	756.9		[15]
Exp.	-	813	762		[21]

Table S8: Measurement and computed IR active mode computed for isomer **1**. ν_s corresponds to the symmetric stretching mode, ν_{as} , to the asymmetric stretching mode and ν_b to the bending mode.

S4.2 Th₂O₄

The minimum energy structure presents a *trans*-type geometry with two of the four oxygen atoms bridging the two thorium atoms and the two other oxygen atoms occupying terminal positions on the thorium atoms, thus leading to an overall C_{2h} symmetry. The Th-O distances in the rhombic ring are 2.18 Å while that for the terminal oxygen atoms are slightly shorter (1.92 Å). The Th-O-Th and O-Th-O angles in the rhombic ring are 105.4 ° and 74.6 °, respectively. These distances and angles are in good agreement with the CCSD(T) values reported by Dixon *et al.* (2.18 Å and 1.90 Å for the Th-O distances, respectively, and 105.1 ° and 74.9 ° for the angles, respectively).¹⁵ Interestingly, for this cluster, two additional stable structures are found 0.12 eV and 0.16 eV higher in energy than the minimum energy structure (Fig. S4). While the first one (isomer **2**) has a capped pseudo-triangular bipyramid geometry, the second one (isomer **3**) corresponds to the *cis* analogue of the minimum energy structure.

Despite being very close in energy, the three isomers have rather different IR signature and DOS features (Fig. S4). For the *trans* isomer, there are three IR active-modes: the first one, at 795 cm⁻¹, corresponds to the anti-symmetric stretching of the terminal oxygen atoms, while the two others, at 600 cm⁻¹ and 473 cm⁻¹, respectively, correspond to rhombus stretching modes. These frequencies are in good agreement with the one reported by Dixon *et al.* for the argon matrix measurements (776 cm⁻¹, 581 cm⁻¹ and 478 cm⁻¹, respectively).¹⁵ For the *cis* isomer, four IR active-modes are identified. Among these, three are identical to that obtained for the *trans* isomer: the anti-symmetric stretching mode at 795 cm⁻¹ and the two rhombus stretching modes at 596 cm⁻¹ and 467 cm⁻¹, respectively. The fourth mode, which is observed at 803 cm⁻¹, corresponds to the symmetric stretching mode of the terminal oxygen atoms, which was forbidden by symmetry in the *trans* isomer. For the bipyramid-like isomer, there is a total of seven active-modes: while the high energy mode at 788 cm⁻¹ is attributed to stretching of the terminal oxygen atom, all the other modes correspond to rhombus stretching in the pseudo-triangular bipyramid.

From the electronic structure perspective, the *cis* and *trans* isomers have very similar DOS (Fig. S4). In both cases, the 2p orbitals of the terminal oxygen make a dominant contribution to the valence orbitals, when the 2p orbitals of the bridging oxygen atoms only contribute to states 1 eV below the Fermi level. In the bipyramid-like isomer, the 2p orbitals of the terminal oxygen still make a dominant contribution to the valence orbitals, but the later is less intense. Also, the 2p orbitals of the bridging oxygen atoms contribute more significantly to states closer to the Fermi level. In all cases, the virtual orbitals dominantly stem from thorium-based orbitals. Yet, the *cis* and *trans* isomers have a very distinct two-peak-shaped virtual orbitals stemming from the Th-7s orbital, compared to bipyramid-like isomer, where the Th-5f and 6d orbitals make a stronger contribution. Interestingly, these DOS have similar features to that of the ThO₂ minimum energy structure (Fig. S3).

S4.3 Th₃O₆

The minimum energy structure has C_s symmetry. It can be described as a six-member ring of alternating thorium and oxygen atoms, where the three thorium atoms are connected through another oxygen atom. Then one thorium atom also holds a terminal oxygen, while

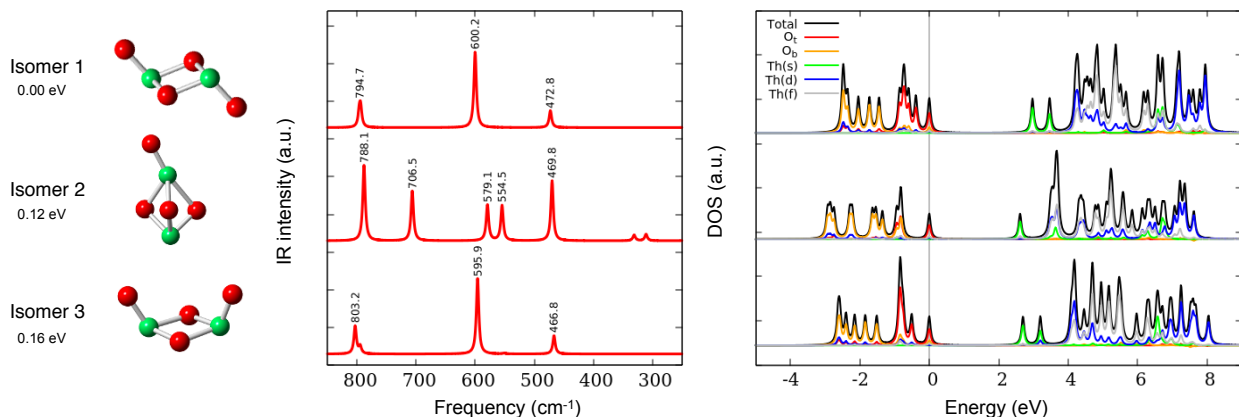


Figure S4: Structure (left), IR spectra (middle) and DOS (right) of the Th₂O₄ lowest energy structure and its two closest isomers (in the DOS, O_t corresponds to the O-2p orbitals of the terminal oxygen atoms, and O_b, to the O-2p orbitals of the bridging oxygen atoms)

the two other thorium atoms are bridged by another oxygen atom (Fig. S5). The Th-O distance for the terminal oxygen is 1.92 Å, similarly to Th₂O₄. The other Th-O distances range from 2.06 Å to 2.39 Å.

For this cluster, our calculations evidence IR-active modes at the following frequencies: 792 cm⁻¹, 649 cm⁻¹, 559 cm⁻¹, 508 cm⁻¹ and 460 cm⁻¹ (Fig. S5). While the first mode corresponds to the stretching of the terminal oxygen atom, the other correspond to rhombus stretching modes. To our knowledge, there is no IR data available for that cluster (or any other bigger cluster studied herein) that could support our findings.

Interestingly, the DOS of this cluster is very close to that of all the minimum energy structures discussed so far, as its valence orbitals dominated by O-2p states and the virtual orbitals, by Th-7s states (Fig. S5). This structure is particularly stable compared to the other Th₃O₆ isomers as it is found about 0.59 eV below the next stable singlet isomer.

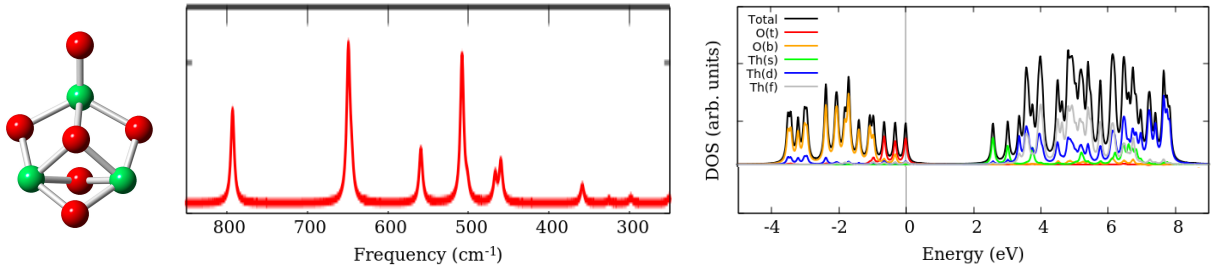


Figure S5: Structure (left), IR spectra (middle) and DOS (right) of the Th₃O₆ lowest energy structure (in the DOS, O_t corresponds to the O-2p orbitals of the terminal oxygen atoms, and O_b, to the O-2p orbitals of the bridging oxygen atoms)

S4.4 Th₄O₈

The lowest energy structure has C_{3v} symmetry. It shows tetrahedral arrangement of the four thorium atoms, with each thorium atom bridged to the others by an oxygen atom, and one oxygen atom also occupying a terminal position (Fig. S6). The Th-O distance for the terminal oxygen is 1.92 Å while the other Th-O distances are ranging from 2.07 Å to 2.46 Å. For this cluster, there are two stable isomers very close in energy: isomer 2 is 0.01 eV higher and energy and isomer 3, 0.06 eV higher (Fig. S6). Both isomers have C_s symmetry and their structure can be described, from the minimum energy structure of the Th₃O₆ cluster, as having an additional ThO₂ unit bridging the two thorium atoms already connected by three oxygen atoms. Into more details, the bridge is achieved such that the additional thorium atom coordinates two of the three bridging oxygen atoms. The most significant difference between the two isomers is the orientation of the terminal oxygen, which differs by about 90 ° between the two isomers. In both cases, the Th-O distance for the terminal oxygen is 1.92 Å while the other Th-O distances range from 2.08 Å to 2.45 Å.

In terms of IR spectroscopy (Fig. S6), all three isomers have a common peak around 785 cm⁻¹, which corresponds to the stretching mode of the terminal oxygen atom, and then two groups of peaks (around 640 cm⁻¹ and 480 cm⁻¹, respectively) which correspond to rhombus modes. Interestingly, for the minimum energy isomer, the group of peaks around 640 cm⁻¹ is noticeably shifted towards higher frequencies, while the peak at about 535 cm⁻¹ is almost completely switched off. This is most likely a consequence of the high symmetry, that forbids certain active modes.

Similarly, noticeable differences are also seen in the DOS (Fig. S6). While valence orbitals of all three isomers are dominated by O-2p states, virtual orbitals of isomer 1 are dominated by Th-7s states, when that of the two other isomers shows a non negligible contribution of the Th-5f and 6d states.

S4.5 Th₅O₁₀

The minimum energy structure has C_{4v} symmetry. The five thorium atoms are arranged in a square pyramid fashion. All oxygen atoms are in bridging position, connecting two to four thorium atoms together, except for one oxygen atom, which holds a terminal position at the top of the pyramid (Fig. S7). The Th-O distance for the terminal oxygen is 1.93 Å while the other Th-O distances range from 2.18 Å to 2.44 Å.

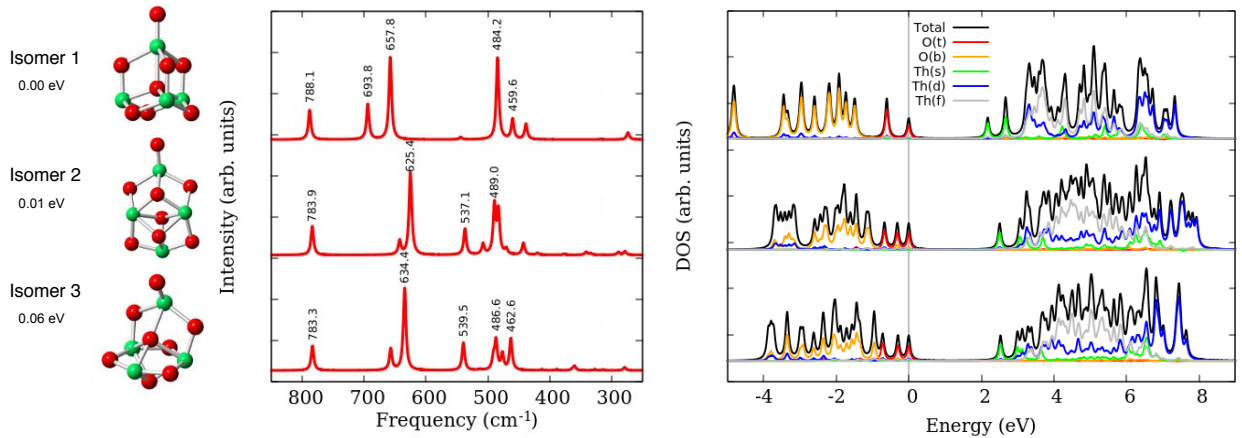


Figure S6: Structure (left), IR spectra (middle) and DOS (right) of the lowest energy Th_4O_8 structure and its two closest isomers (in the DOS, O_t corresponds to the O-2p orbitals of the terminal oxygen atoms, and O_b , to the O-2p orbitals of the bridging oxygen atoms)

For this cluster, due to the high symmetry, 18 IR-active modes are expected, out of which 8 belong to the A_1 irreducible representation (distortion along the z direction associated to the terminal oxygen) and 10 belong to the E irreducible representation (distortion in the transverse plan). From our calculations (Fig. S7), only 4 modes have appreciable intensity, two of which belong to the A_1 irreducible representation (771 cm^{-1} and 510 cm^{-1}), while the two other belong to the E irreducible representation (620 cm^{-1} and 512 cm^{-1}).

The DOS of this cluster (Fig. S7) is very close to that of all the minimum energy structures discussed so far, as its valence orbitals are dominated by O-2p states and its virtual orbitals, by Th-7s states. Also, similarly to Th_3O_6 , this structure is particularly stable compared to the other isomers, as the next stable singlet isomer is found 0.24 eV higher in energy.

S4.6 Th_6O_{12}

As the Th_6O_{12} lowest energy structure is discussed in details in the last section of the main text, it is not discussed here.

S4.7 Th_7O_{14}

The minimum energy structure has C_1 symmetry. Despite some similarities with the Th_6O_{12} minimum energy structure, the Th_7O_{14} lowest energy structure presents noticeable distortions (Fig. S9). In the Th_7O_{14} cluster, the Th-O distances range from 2.11 \AA to 2.52 \AA . Interestingly, there are two additional stable isomers less than 0.05 eV higher in energy, among which one has higher C_s symmetry, and the other C_1 symmetry.

For the three isomers, the IR-active modes are separated into two groups of peaks, with one group ranging from 690 cm^{-1} to 600 cm^{-1} and the other, from 520 cm^{-1} to 420 cm^{-1} (Fig. S9). There is no clear difference between the IR spectra of these three isomers, which makes it complicated to dissociate the isomers from each other experimentally.

The same conclusion arises from the electronic structure perspective. Indeed, for all three isomers, the DOS shows valence orbitals dominated by O-2p states and virtual orbitals

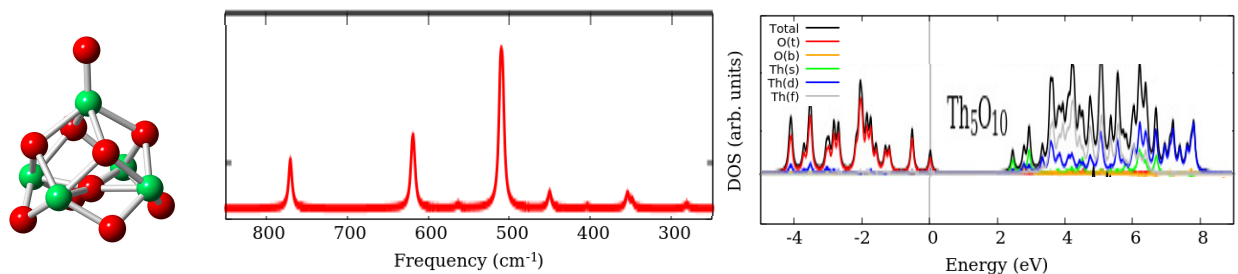


Figure S7: Structure (left), IR spectra (middle) and DOS (right) of the Th_5O_{10} lowest energy structure (in the DOS, O_t corresponds to the O-2p orbitals of the terminal oxygen atoms, and O_b , to the O-2p orbitals of the bridging oxygen atoms)

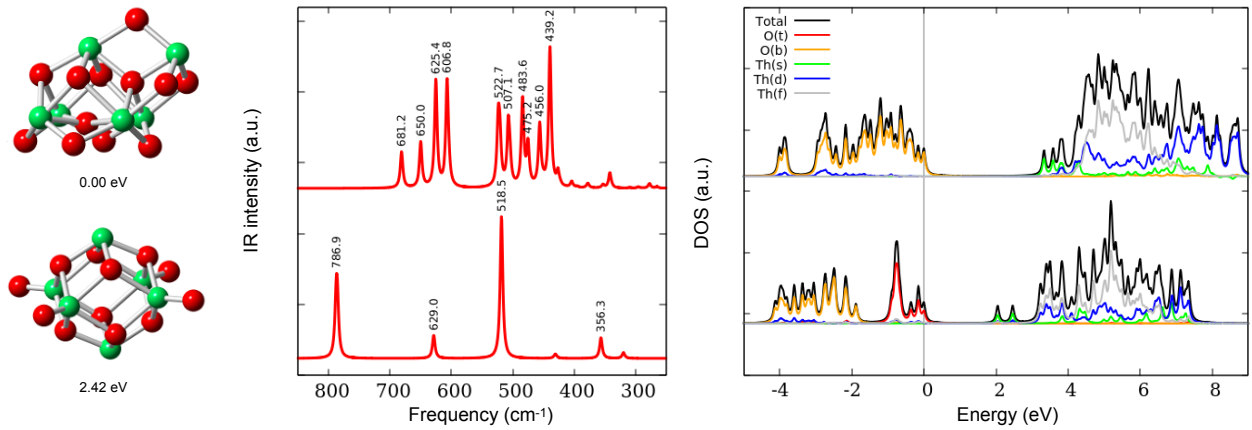


Figure S8: Structure (left), IR spectra (middle) and DOS (right) of the Th_5O_{12} lowest energy structure together with the structure by Shamov²² (in the DOS, O_t corresponds to the O-2p orbitals of the terminal oxygen atoms, and O_b , to the O-2p orbitals of the bridging oxygen atoms)

dominated by Th-7s states (Fig. S9).

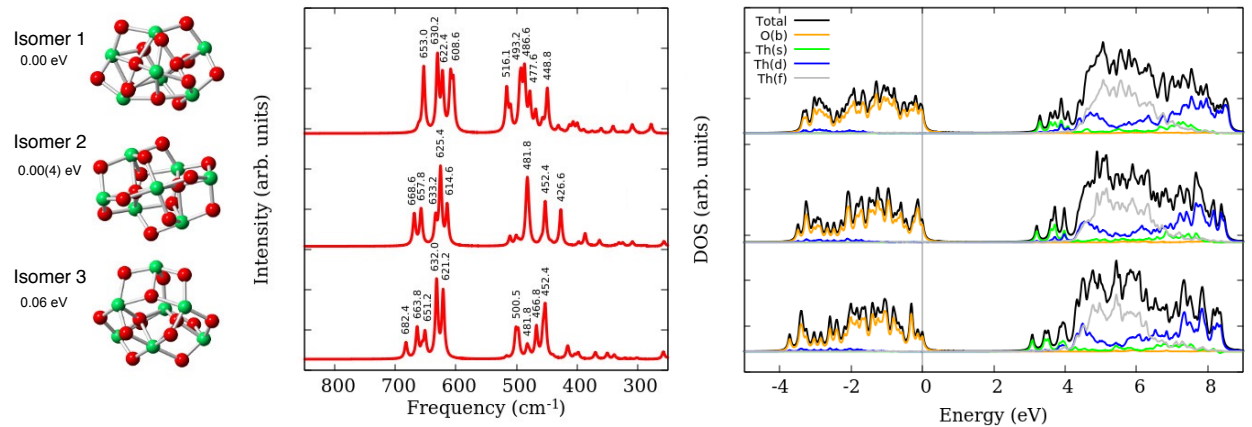


Figure S9: Structure (left), IR spectra (middle) and DOS (right) of the lowest energy Th_7O_{14} structure and its two closest isomers (in the DOS, O_t corresponds to the O-2p orbitals of the terminal oxygen atoms, and O_b , to the O-2p orbitals of the bridging oxygen atoms)

S4.8 Th_8O_{16}

The minimum energy structure has C_s symmetry (Fig. S10). It is very similar to the minimum energy structure obtained for Th_7O_{14} , with an additional ThO_2 unit grafted under the base of the square pyramid left (from Th_5O_{10} and on). In this cluster, the Th-O distances range from 2.14 Å to 2.53 Å.

Our calculations evidence IR-active modes at the following frequencies (Fig. S10): 684 cm^{-1} , 663 cm^{-1} , 651 cm^{-1} , 625 cm^{-1} , 603 cm^{-1} , 597 cm^{-1} , 510 cm^{-1} , 493 cm^{-1} , 475 cm^{-1} , 456 cm^{-1} , 452 cm^{-1} and 447 cm^{-1} .

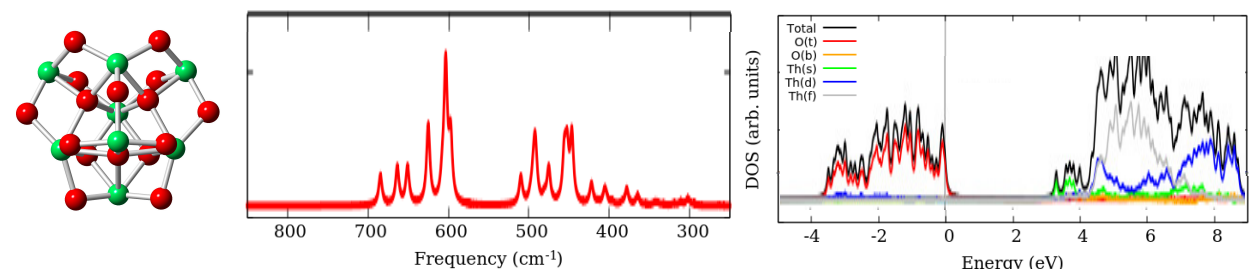


Figure S10: Structure (left), IR spectra (middle) and DOS (right) of the Th_8O_{16} lowest energy structure (in the DOS, O_t corresponds to the O-2p orbitals of the terminal oxygen atoms, and O_b , to the O-2p orbitals of the bridging oxygen atoms)

Interestingly, the DOS of this cluster is very close to that of all the minimum energy structures discussed so far, as its valence orbitals are dominated by O-2p states and virtual orbitals, by Th-7s states (Fig. S10). Also, similarly to Th₃O₆ and Th₅O₁₀, this structure is particularly stable compared to the other isomers, as the next stable singlet isomer is found almost 0.5 eV higher in energy.

S5 Stable isomers for the $[\text{Th}_6(\text{OH})_4(\text{O})_4(\text{O})_6]$ cluster

Table S9 shows the structure and relative energy of two $[\text{Th}_6(\text{OH})_4(\text{O})_4(\text{O})_6]$ isomer. The first one (left) is built from the lowest energy structure of the Th_6O_{12} cluster series by adding two oxygen atoms and four hydrogen atoms (Fig. S11). The other isomer (right) corresponds to the model system **6A** by Knope *et al.*²³ which is the lowest energy isomer among the different models studied in their work. Both structures were optimized at the DFT level of theory using the same approach as detailed in section S1.2.

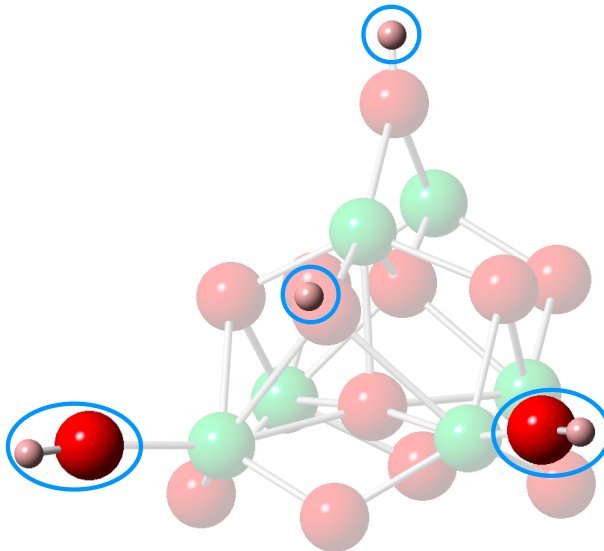
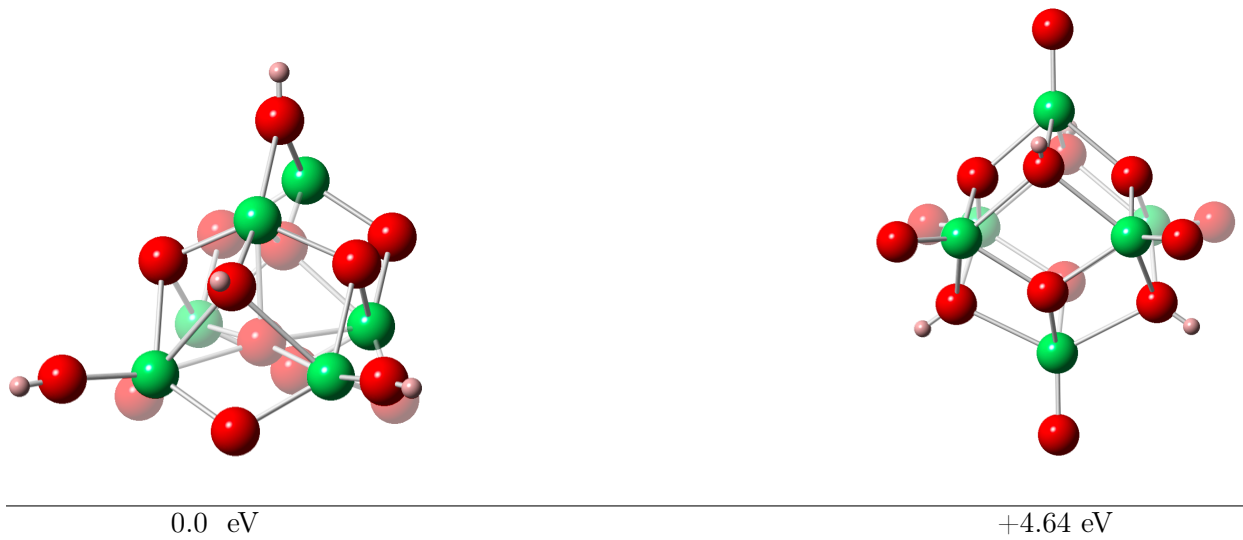


Figure S11: Structure of the $[\text{Th}_6(\text{OH})_4(\text{O})_4(\text{O})_6]$ isomer built from the Th_6O_{12} lowest energy structure, with respect to the latter structure

Table S9: Structure and relative energy of two $[\text{Th}_6(\text{OH})_4(\text{O})_4(\text{O})_6]$ isomers



References

- [1] E. J. Baerends, T. Ziegler, A. J. Atkins, J. Autschbach, D. Bashford, O. Baseggio, A. Bérces, F. M. Bickelhaupt, C. Bo, P. M. Boerritger, L. Cavallo, C. Daul, D. P. Chong, D. V. Chulhai, L. Deng, R. M. Dickson, J. M. Dieterich, D. E. Ellis, M. van Faassen, A. Ghysels, A. Giammona, S. J. A. van Gisbergen, A. Goez, A. W. Götz, S. Gusarov, F. E. Harris, P. van den Hoek, Z. Hu, C. R. Jacob, H. Jacobsen, L. Jensen, L. Joubert, J. W. Kaminski, G. van Kessel, C. König, F. Kootstra, A. Kovalenko, M. Krykunov, E. van Lenthe, D. A. McCormack, A. Michalak, M. Mitoraj, S. M. Morton, J. Neugebauer, V. P. Nicu, L. Noodleman, V. P. Osinga, S. Patchkovskii, M. Pavanello, C. A. Peeples, P. H. T. Philipsen, D. Post, C. C. Pye, H. Ramanantoanina, P. Ramos, W. Ravenek, J. I. Rodríguez, P. Ros, R. Rüger, P. R. T. Schipper, D. Schlüns, H. van Schoot, G. Schreckenbach, J. S. Seldenthuis, M. Seth, J. G. Snijders, M. Solà, S. M., M. Swart, D. Swerhone, G. te Velde, V. Tognetti, P. Vernooijs, L. Versluis, L. Visscher, O. Visser, F. Wang, T. A. Wesolowski, E. M. van Wezenbeek, G. Wiesenekker, S. K. Wolff, T. K. Woo and A. L. Yakovlev, *ADF2017, SCM, Theoretical Chemistry, Vrije Universiteit, Amsterdam, The Netherlands*, <https://www.scm.com>, 2017.
- [2] G. te Velde, F. M. Bickelhaupt, E. J. Baerends, C. Fonseca Guerra, S. J. A. van Gisbergen, J. G. Snijders and T. Ziegler, *Journal of Computational Chemistry*, 2001, **22**, 931–967.
- [3] C. Fonseca Guerra, J. G. Snijders, G. te Velde and E. J. Baerends, *Theoretical Chemistry Accounts: Theory, Computation, and Modeling (Theoretica Chimica Acta)*, 1998, **99**, 391–403.
- [4] J. P. Perdew, *Physical Review B*, 1986, **33**, 8822–8824.
- [5] A. D. Becke, *Physical Review A*, 1988, **38**, 3098–3100.
- [6] E. van Lenthe, E. J. Baerends and J. G. Snijders, *The Journal of Chemical Physics*, 1993, **99**, 4597–4610.
- [7] E. van Lenthe, E. J. Baerends and J. G. Snijders, *The Journal of Chemical Physics*, 1994, **101**, 9783–9792.
- [8] E. van Lenthe, A. Ehlers and E.-J. Baerends, *The Journal of Chemical Physics*, 1999, **110**, 8943–8953.
- [9] F. Neese, *Wiley Interdisciplinary Reviews: Computational Molecular Science*, 2017, **8**, e1327.
- [10] F. Weigend, F. Furche and R. Ahlrichs, *The Journal of Chemical Physics*, 2003, **119**, 12753–12762.
- [11] F. Weigend and R. Ahlrichs, *Phys. Chem. Chem. Phys.*, 2005, **7**, 3297–3305.
- [12] D. A. Pantazis and F. Neese, *Journal of Chemical Theory and Computation*, 2011, **7**, 677–684.
- [13] W. R. Wadt, *Journal of the American Chemical Society*, 1981, **103**, 6053–6057.
- [14] H. Xiao, H.-S. Hu, W. H. E. Schwarz and J. Li, *The Journal of Physical Chemistry A*, 2010, **114**, 8837–8844.
- [15] L. Andrews, Y. Gong, B. Liang, V. E. Jackson, R. Flamerich, S. Li and D. A. Dixon, *The Journal of Physical Chemistry A*, 2011, **115**, 14407–14416.
- [16] L. Andrews, M. Zhou, B. Liang, J. Li and B. E. Bursten, *Journal of the American Chemical Society*, 2000, **122**, 11440–11449.
- [17] K. G. Dyall, *Molecular Physics*, 1999, **96**, 511–518.

- [18] G. M. Kibler, T. F. Lyon, M. J. Linevski and V. J. DeSantis, *Refractory Material Research*, Air force materials laboratory - research and technology division - air force systems command - wright-patterson air force base, ohio, usa technical report, 1964.
- [19] S. D. Gabelnick, G. T. Reedy and M. G. Chasanov, *The Journal of Chemical Physics*, 1974, **60**, 1167–1171.
- [20] M. Zhou and L. Andrews, *The Journal of Chemical Physics*, 1999, **111**, 11044–11049.
- [21] A. Kovács and R. J. Konings, *The Journal of Physical Chemistry A*, 2011, **115**, 6646–6656.
- [22] G. A. Shamov, *Inorganic Chemistry*, 2012, **51**, 6507–6516.
- [23] K. E. Knope, R. E. Wilson, M. Vasiliu, D. A. Dixon and L. Soderholm, *Inorganic Chemistry*, 2011, **50**, 9696–9704.